Hierarchical Gold Flower with Sharp Tips from Controlled Galvanic Replacement Reaction for High Surface Enhanced Raman Scattering Activity

ARTICLE *in* THE JOURNAL OF PHYSICAL CHEMISTRY C · NOVEMBER 2012

Impact Factor: 4.77 · DOI: 10.1021/jp306330p

4 AUTHORS, INCLUDING:

Mukul Pradhan
Pohang University of Science and Technology
45 PUBLICATIONS **755** CITATIONS
SEE PROFILE

Joydeep Chowdhury
Jadavpur University
71 PUBLICATIONS **631** CITATIONS
SEE PROFILE

Arun Kumar Sinha
Seoul National University
11 PUBLICATIONS **123** CITATIONS
SEE PROFILE

THE JOURNAL OF PHYSICAL CHEMISTRY C

Article

pubs.acs.org/JPCC

Hierarchical Gold Flower with Sharp Tips from Controlled Galvanic Replacement Reaction for High Surface Enhanced Raman Scattering Activity

Mukul Pradhan,[†] Joydeep Chowdhury,[‡] Sougata Sarkar,[†] Arun Kumar Sinha,[†] and Tarasankar Pal*[,†]

[†]Department of Chemistry, Indian Institute of Technology, Kharagpur-721302, India

[‡]Department of Physics, Sammilani Mahavidyalaya, Baghajatin Station, E.M. Bypass, Kolkata 700075, India

Supporting Information

ABSTRACT: Highly branched Au flowers (AuFs) with sharp tips have been synthesized in high yield by controlling the kinetics of nanocrystal growth via galvanic replacement reaction. Controlled galvanic replacement takes place on appropriately chosen commercially available polystyrene bead supported Cu nanoparticles with $HAuCl_4$. Such a reaction is thermodynamically driven through the exploitation of a Cu(II)/Cu(0) redox couple during nanocrystal formation. The hierarchical morphology of the resulting naked Au flowers (AuFs) depends on the galvanic exchange rate, which increases with increasing $HAuCl_4$ concentration but over a specific concentration range. The formation of AuF is carefully studied, and a spontaneous assembly mechanism is proposed. The time-course experimental results show that the influence of electrostatic field force (EFF) of the charged resin beads is held responsible for prickly tipped AuF formation. Then the fabrication of AuF morphology becomes a large-scale free-standing synthetic protocol for a chemically stable substrate for surface-enhanced Raman scattering (SERS) studies down to the single molecular level. The SERS results guarantee that the as-prepared naked AuF is an excellent and stable SERS substrate. The prickly tips of the gold bearing enhanced field with a large number of embedded "hot spots" hidden within the oriented petals and absence of surfactant or capping agent invites a probe molecule to show the enhancement even for a concentration of 4-mercaptopyridine (4-MPy) down to 10^{-12} mol dm^{-3}. The electric field distribution around the hot spot has been estimated from 3D-FDTD simulation studies. The selective enhancements of SER bands of the 4-MPy molecule have been unveiled from the view of Herzberg–Teller (HT) charge transfer (CT) mechanism.

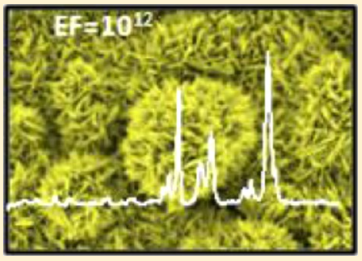

INTRODUCTION

Noble metal nanostructures have been extensively studied due to their fascinating optical,[1] electronic,[2] and catalytic[3] properties. Great efforts have been devoted to control the size and shape of gold nanocrystals,[4] because it is well established that their properties are size- and shape-dependent. Among them, gold NFs have attracted special interest in recent years[5] due to pronounced electromagnetic field effect surrounding NFs, which may provide a new chance to extend the applications of gold nanocrystals in surface enhanced Raman scattering (SERS)[6] and catalysis.[7] To obtain high-quality SERS response down to the single molecular level,[8] we need clean surface devoid of surface capping. Up to date there are very few reports to obtain exclusively high quality flowerlike naked morphology from gold. Galvanic replacement reaction offers a versatile and quantitative route to fabricate metal nanostructures with controllable hollow interiors and porous walls with a clean surface without any capping agent.[9] Sun et al. have observed the chemical transformation of solid Ag nanowires into nanotubes of Au or Au–Ag alloy from galvanic replacement reaction.[10] Similarly, Pt or Pd with a Au precursor has been tried by Skrabalak et al.[11] for tetrapodal and star-shaped[12] decahedral Au structures.

Nanostructures of gold have been of great promise due to their chemical stability, good biocompatibility, and strong SERS enhancement. It is established that the huge signal improvement in SERS arises from the electromagnetic enhancement at the "hot spots", which may be either in the interstitial voids or intersections or high radii of curvature of the metal structures.[13] Experimental measurements[14] and theoretical calculations[15] have revealed that the strong enhancement of the electromagnetic field in complex gold nanostructures such as multipods, dendrites, and NFs are due to innumerable "hot spots" on a single nanoparticle assembly. Chen et al. developed a colloid chemical synthetic protocol using cetyltrimethylammonium bromide (CTAB) as a capping agent.[16] However, this method can only produce multipod gold nanostructures with only a few tips. Recently, Xie et al. reported the synthesis of highly branched (>10 tips) gold NFs, and they modified those gold NFs as SERS-active tags with polymers.[17] Multibranched (~6 tips) gold nanoparticles were first presented by Sau et al. and star-shaped gold nanoparticles were obtained by reducing $HAuCl_4$ with CTAB in presence of gold seeds.[18] The used

Received: June 27, 2012
Revised: October 19, 2012
Published: October 26, 2012

Scheme 1. Galvanic Replacement of Cu(0) by $AuCl_4^-$ for AuF Formation under Weak EFF for Single Molecule SERS Detection

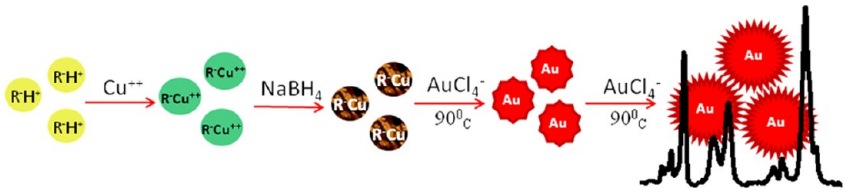

surfactant limits gold nanostars in SERS application because surfactant debars Raman probes to get adsorbed on the surface of gold nanoparticles causing weak SERS signals.

Herein, we report for the first time a simple method to fabricate highly branched gold NFs with abundant petal-shaped tips exploiting galvanic exchange of polystyrene bead supported Cu (prepared by $NaBH_4$ reduction) nanoparticle with $HAuCl_4$ at ~90 °C (Scheme 1). It has been concluded that the growth of gold NFs follows a classical growth pattern under electrostatic field force (EFF), which differs from other reported "aggregation" growth processes.[19] As-synthesized gold NFs provide a clean surface with enhanced electric field, as visualized through three-dimensional finite difference time domain (3D-FDTD) simulations, where Raman probe 4-mercaptopyridine (4-MPy) molecule gets adsorbed without any hindrance. The NF of Au has performed best in terms of SERS sensitivity while compared with gold nanospheres. The genesis of selective enhancement of the Raman band of 4-MPy molecule adsorbed on as prepared AuF surface are also explored in terms of Herzberg–Teller (HT) charge transfer (CT) contribution.

EXPERIMENTAL SECTION

1. Experimental Details. *1.1. Chemicals and Materials.* Hydrogen tetracholoroauric acid ($HAuCl_4 \cdot 3H_2O$), Cation exchange resin (Seralite SRC-120), sodium borohydride, and 4-mercaptopyridine molecules were received from Sigma Aldrich. Copper sulfate ($CuSO_4$) was obtained from Merck. All chemicals were used without further purification and solutions were prepared using double distilled water.

1.2. Syntheses of Gold Flower. 1.2.1. Synthesis of Resin Immobilized Cu Nanoparticle. Cu(II) precursor ions (0.1 M and 20 mL $CuSO_4$) are allowed to exchange with H^+ ions of the wet cation-exchange resin beads (80 mg R^-H^+) in water with occasional stirring and are kept overnight for complete exchange. The resin beads, on which copper precursor ions are immobilized, are washed several times with water to drain out the unexchanged species. Spherical Cu nanoparticles on the resin beads are grown out of the resin-bound Cu(II) using sodium borohydride as reducing agent. In a typical preparation, resin-bound Cu(II) is mixed with a solution containing 50 mg borohydride (in 10 mL) in a 50 mL beaker. Then, the above mixture is allowed to age for 1 h under ambient conditions. Shiny metallic Cu colored resin beads indicate the formation of Cu nanoparticles. The as-prepared nanoparticles are washed with plentiful hot water. The Cu(0) nanoparticle is not pyrophoric in air; however, upon extended exposure, slow oxidation is observed in air. So the beads with Cu(0) nanoparticle are washed with hot water to avoid oxidation by dissolved oxygen and are used immediately.

1.2.2. Synthesis of Resin Immobilized Gold Flower. AuFs were synthesized under hydrothermal conditions or at room temperature conditions from polystyrene bead stabilized Cu(0) nanoparticle and $HAuCl_4$ solution. A quantitative, simple, and convenient galvanic replacement method evolves gold flower onto the resin beads, which looks like a carnation flower. Simple manipulation of 100 mg resin immobilized Cu(0) nanoparticle is transferred to a solution containing 4 mL of 10^{-2} M $HAuCl_4$ and is kept at room temperature for 12 h. In another set, the same amount of Cu(0) and 4 mL of 10^{-2} M $HAuCl_4$ are taken in a screw-capped test tube and heated on a water bath for 2 h to grow the AuF assemblies on the resin beads. Simple sonication detaches the AuFs from the resin bead surfaces.

1.2.3. Procedure for SERS Measurement. Fresh stock solutions of 4-mercaptopyridine were prepared regularly in water with variable concentrations (10^{-6} mol dm^{-3} – 10^{-12} mol dm^{-3}). To test the performance of our nanostructured SERS substrates, a dilute dispersion of Au flower (10 μmol/L in water) and 55 nm Au nanosphere (100 μmol/L in water) were separately incubated for 12 h. All SERS spectra were recorded dispensing 30 μL of the incubated solution on an aluminum foil.

1.3. Instrumentation. XRD was done in a PW1710 diffractometer, a Philips, Holland, instrument. The XRD data are analyzed using JCPDS software. FESEM analysis is done with a supra, Carl Zeiss Pvt. Ltd. instrument and an EDAX machine (Oxford link and ISIS 300) attached to the instrument is used to obtain the nanocrystal morphology and composition. TEM analysis is done with an instrument H-9000 NAR, Hitachi, using an accelerating voltage of 300 kV. SERS spectra are obtained with a Renishaw Raman Microscope, equipped with a He–Ne laser excitation source emitting at a wavelength of 633 nm, and a Peltier cooled (−70 °C) charge coupled device (CCD) camera. A Leica microscope with 50× objective lens is used. The holographic grating with 1800 grooves/mm and the 1 cm^{-1} slit enabled the spectral resolution. Laser power at the sample is 12 mW and the data acquisition time is 30 s. The absorption spectra of the 4-MPy molecule in aqueous and in DMSO, ethanol, and toluene solvents have been recorded using SPECTRASCAN UV 2600 digital spectrophotometer (Chemito, India).

Computational Details. The three-dimensional finite difference time domain (3D-FDTD) simulation technique[20] has been applied to simulate the spatial distribution of the electric field around gold nano tips. A representative section of the as synthesized NF containing five gold nano tips each of 100 nm length with 20 and 5 nm base and apex radii, respectively, have been considered for the simulation. The dispersive property of the gold nano material has been incorporated in the simulation run using the generalized Drude model. The complex permittivity $\varepsilon(\omega)$ according to the generalized Drude model is represented as

$$\varepsilon(\omega) = \varepsilon_\infty + \frac{\varepsilon_s - \varepsilon_\infty}{1 + i\omega\tau} + \frac{\sigma}{i\omega\varepsilon_0} \quad (1)$$

where ε_s, ε_∞, σ, and τ represent static permittivity, infinite frequency permittivity, conductivity, and the relaxation time,

dx.doi.org/10.1021/jp306330p | J. Phys. Chem. C 2012, 116, 24301–24313

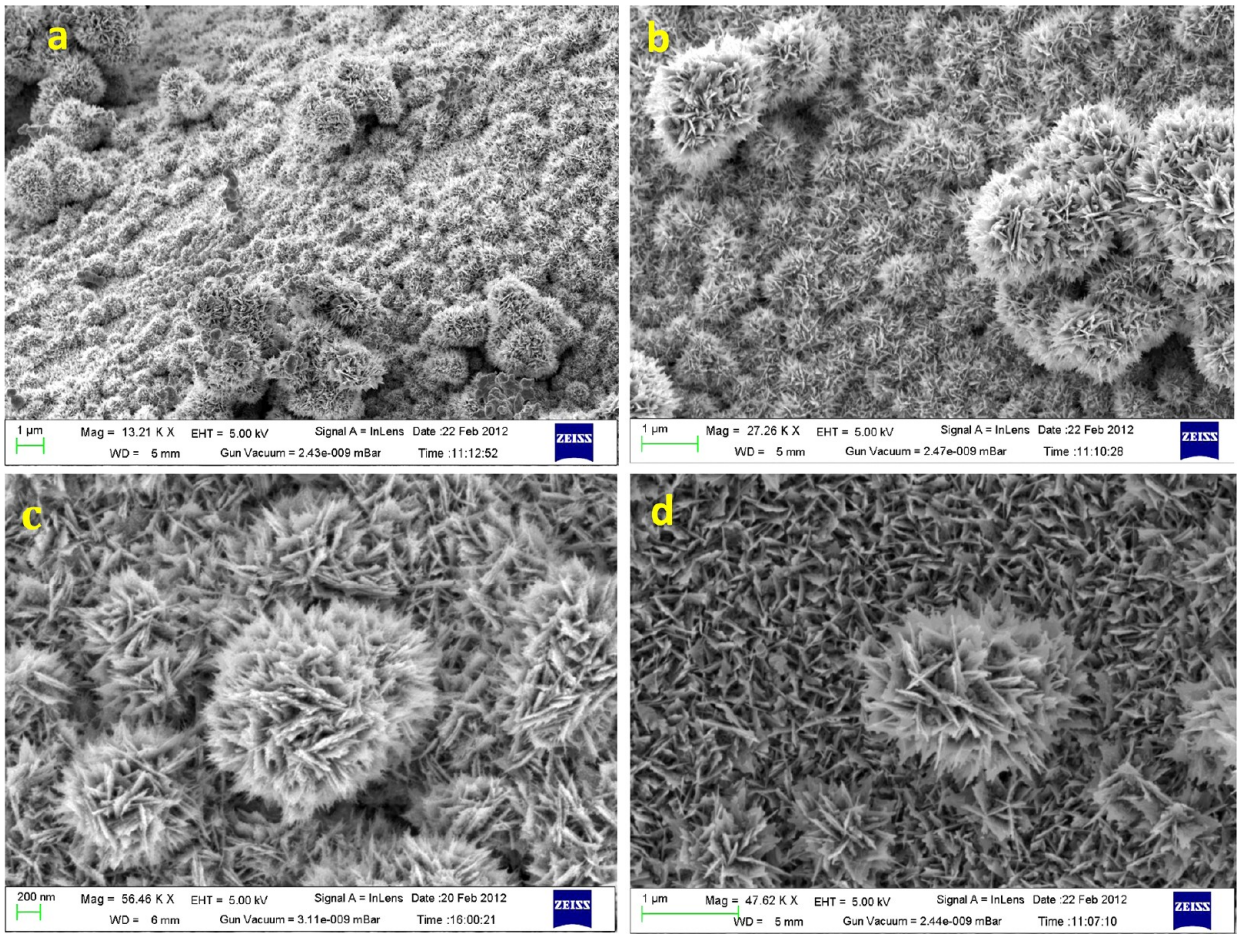

Figure 1. FESEM images at different magnification (a–d) of Au flowers at moderate (4 mL of 10^{-2} M $HAuCl_4$ and 80 mg resin immobilized Cu(0) nanoparticle) $HAuCl_4$ concentration on water bath at 90 °C.

respectively, ω is the angular frequency, and ε_0 is the permittivity of free space. The four parameters ε_s, ε_∞, σ, and τ are then adjusted through curve fitting technique to match the complex permittivity correctly. The complex permittivity $\varepsilon(\omega)$, as obtained from the generalized Drude model, faithfully represents the optical response of the metallic nanomaterials over a wide frequency range, thereby ensuring the accuracy of the FDTD simulation.[20,21]

The Yee cell used in the calculation was set at $1 \times 1 \times 1$ nm^3 and the step size was fixed at 1.73 atto second. The number of periods of the incident sinusoidal wave was fixed at 11 to ensure the convergence of the calculation. The amplitude of the incident sinusoidal wave was set at 1 V/m for the excitation wavelength of 632.8 nm. The 3D-FDTD calculations were performed using XFDTD 6.3 software [RemCom XFDTD 6.3].

The theoretically simulated absorption spectrum of the molecule in aqueous solvent medium has been estimated by calculating the Franck–Condon transition energies for the B3LYP/aug-cc-PVTZ optimized ground state structures at the TD DFT B3LYP/aug-cc-PVTZ level of theory. The solvent effects on the structure of the molecule were estimated by the integral equation formalism polarized continuum model (IEFPCM), which is a special version of the polarized continuum model (PCM). In this model, the solvent is treated as a continuum dielectric medium and the solute is considered as a trapped molecule in a cavity surrounded by the solvent. Detail discussions of the IEFPCM model have been reported elsewhere.[22]

RESULTS AND DISCUSSION

The shape, size, and composition of the as-synthesized Au flowers were characterized by SEM, TEM (Figures 1–4), and EDS analysis (Supporting Information, Figures 1 and 2). Figure 3 shows the presence of abundant carnation flower shaped structures. The tips of the AuFs are within 5–20 nm range, which is different from the reported AuFs of poor stability.[23] TEM images of AuFs further confirm that the flowers bear (Figure 2b,c) small fine tips with outwardly directing petals. The Au nanostructure is mainly composed of {111} planes with a *d*-spacing of 0.234 nm (Figure 2d). X-ray diffraction pattern (Supporting Information, Figure 3) gives further support to the phase structure of the AuFs without crystallographic impurities. An overwhelmingly strong diffraction peak at 38.09° is assigned to the {111} facets of a face-centered cubic metal gold structure, while the diffraction peaks of the other four facets are weak (JCPDS file number 04-0784). Usually, Au nanoparticles bearing hierarchical structures show strong bands in the 650–900 nm wavelength range.[24] The UV–visible extinction spectrum (DRS) of Au flowers in the present case shows an ill-defined SPR band with a small hump due to the scattering of the large flowery structure with ample tips.

It has already been mentioned that the introduction of a resin-supported Cu(0) nanoparticle was essential for the

dx.doi.org/10.1021/jp306330p | J. Phys. Chem. C 2012, 116, 24301–24313

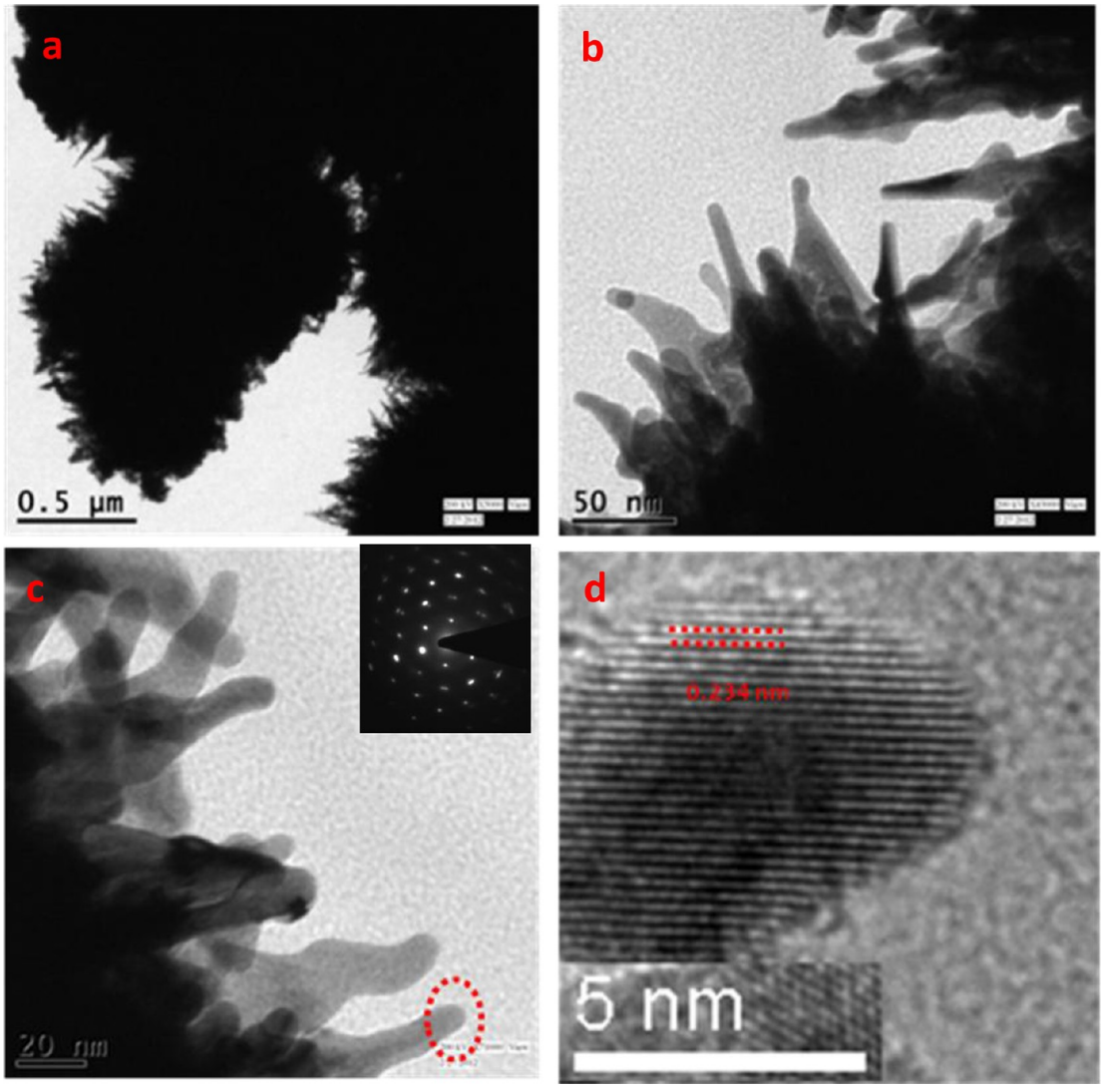

Figure 2. TEM (a–c), SAED (c inset), and HRTEM (d) images of gold flowers.

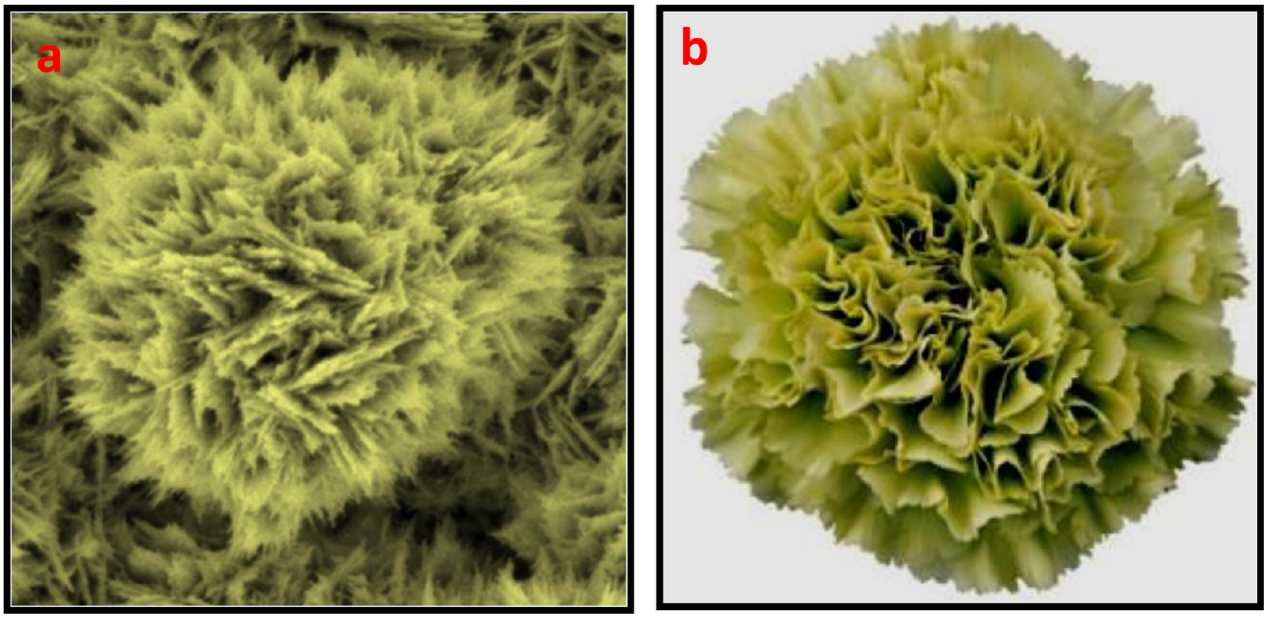

Figure 3. FESEM images of Au flower (a) and digital photograph of natural carnation flower (b).

dx.doi.org/10.1021/jp306330p | J. Phys. Chem. C 2012, 116, 24301–24313

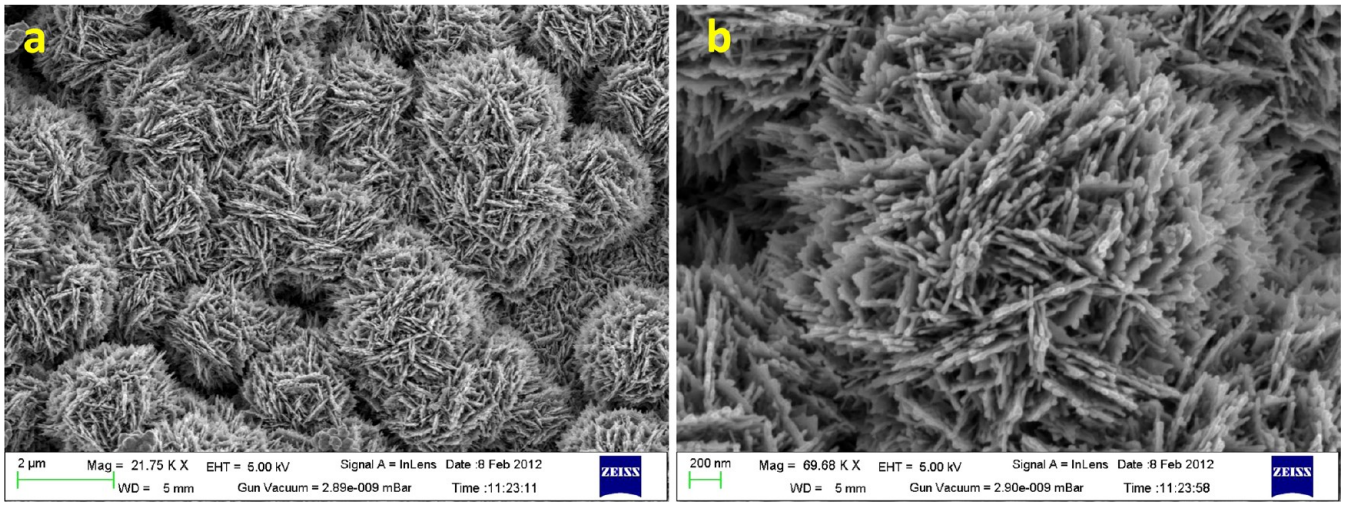

Figure 4. FESEM images at different magnification (a, b) of Au flowers at moderate (4 mL of 10^{-2} M $HAuCl_4$ and 80 mg resin immobilized Cu(0)) $HAuCl_4$ concentration under hydrothermal condition at 110°c.

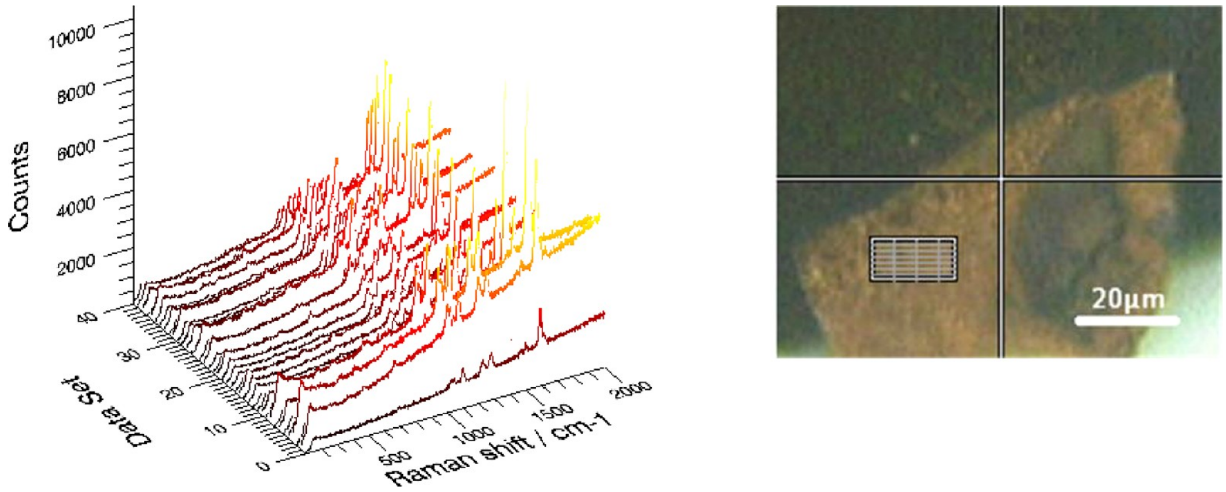

Figure 5. Area mapping of SERS signal on the synthesized AuF substrate with 4-MPy (10^{-9} M).

synthesis of highly branched naked AuFs. Interestingly, Cu(0) escapes out of the Au(0) nanostructures as soluble Cu^{2+} (E^0, 0.34 V) ions imparting a blue color shade to the solution. In the solution phase, $HAuCl_4$ oxidizes Cu(0) and in turn gets reduced to metallic gold. After the completion of galvanic replacement reaction, addition of a fresh batch of $HAuCl_4$ solution did not produce any blue solution. Thus, Cu incorporation in the final AuF structure becomes redundant. Again, unsupported Cu(0), Fe(0), or other metallic nanoparticles (in dispersion) having a similar redox criteria could not fetch AuFs through the obvious galvanic replacement. As soon as the resin immobilized Cu(0) was brought in, Au(III) ions were reduced to gold atoms (E^0, 1.692 V) and then a large number of Au(0) nuclei stuck to the resin surface. Here solid resin surface favors the observed nucleation. When the concentration of gold atoms was large enough, growth rate was migration dominated instead of diffusion related phenomenon. As a result, the effect of anisotropic growth was minimized and the intermediates with a quasi-spherical core and tiny tips were identified. As the nucleation step consumed the initial species in large amounts, the concentration of Au(III) decreased. At this stage, diffusion control reaction dominated, generating small petals of gold nanoparticles. The progress of the reaction results in a slow generation of gold atoms, which seems to be an important criterion for the flowery growth of Au structure. After that, the diffusion control process induces anisotropic growth of the intermediates. At this stage, tips grew larger and broader, generating well-featured gold NFs. The most interesting part of our discovery lies with the inherent stability of the naked AuFs. The stable AuF substrate even if it is 2 months old showed reproducible SERS signal (Figure 5). However, the SERS signal starts decreasing slowly after 3 months (Supporting Information, Figure 4). The formation of carnation flower like assembly resulted in by the successful exploitation of controlled galvanic exchange reaction (Figure 6a–d). The control came from the EFF exerted by the resin moiety.

At the first instance, it is easy to rationalize that simple solution phase galvanic exchange between Cu(0) and $AuCl_4^-$ should be a thermodynamic controlled fast reaction and bulk Au(0) would be the precipitate. In the present case this is not observed, instead carnation flowers from Au particles appeared. The resin bound Cu(0) control the electron exchange and the control came from the negatively charged micrometer size resin beads. One can argue that there should exists columbic repulsion between the negatively charged resin bound Cu(0)

dx.doi.org/10.1021/jp306330p | J. Phys. Chem. C 2012, 116, 24301–24313

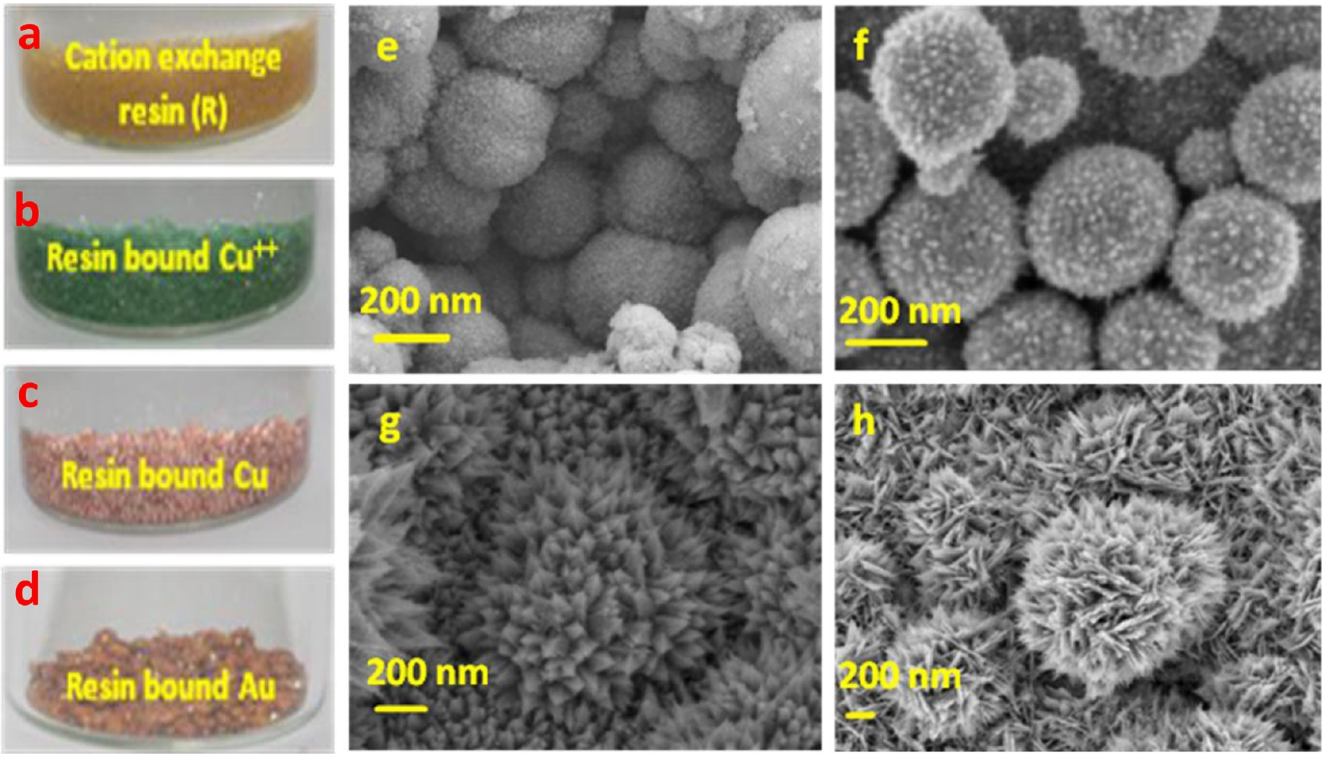

Figure 6. Growth of AuFs after 20, 40, 90, and 120 min (e–h, respectively) of galvanic reaction on resin beads (a–d).

and $AuCl_4^-$. But the product, AuFs stands along and truly rationalizes the observed reaction. The reaction presumably occurs due to strong polarization effect of the two interacting species: resin bound Cu(0) and $AuCl_4^-$ and that is certainly under the control of EFF of the resin beads.

The prickly tipped Au flower formation is observed under surfactant less condition. Surfactant due to their face selective capping may bring directional growth of particle. There happens habitual and template directed growth for the particles. On the other hand, galvanic replacement is a unique way to obtain metal nanoparticle. Thermodynamics makes the process quantitative when there is no kinetic barrier of surfactant, polymer, opposing dielectric medium, and so on. In the present situation, galvanic replacement and EFF cojointly evolve astonishing morphology of AuF. Galvanic reaction produces Au atom from Au(III) ions. The bulk solution supplies Au(III) ions and in turn Cu(II) ion passes into solution. As a result Au(0) is deposited onto the resin surface replacing copper metal. Under normal condition galvanic replacement brings morphology of the particle, which complies with the habitual growth process. However, the negatively charged resin bead directs the incoming atom to get deposited one after the other under the prevailing low temperature (~80 °C) condition. This is caused presumably due to the polarization effect.[25] This polarization effect induced by the charged resin beads fall off and that is inversely proportional to the distance, that is, polarization is maximum for the first layer of deposited Au(0) and minimum at the prickly tips. Thus, the base of the petals becomes wider and at the end sharp tips are found. So, galvanic replacement and EFF evolve flowers with prickly tips.

AuF formation is a consequence of Cu(0)/Au(III) reaction. It was observed that the amount of Cu(0) readily influenced the shape of AuF formation. To confirm it, we maintained $HAuCl_4$ concentration fixed in three different sets of reaction. Typically, in three screw-capped test tubes, we took 30, 80, and 300 mg resin-bound Cu(0) and 4 mL of 10^{-2} M $HAuCl_4$ in each. Then all three test tubes were heated to ~90 °C for 2 h on a water bath. Flower formation was observed only from the second set. In set 1 we observed the anisotropic growth of nanocrystals but no significant amount of flower formation took place (Supporting Information, Figure 5a). For the third set, that is, with the highest amount of Cu(0) we observed the formation of CuO nanocubes along with a few AuF (Supporting Information, Figure 5b). Optimum amount of resin supported Cu(0) was only needed for the formation of AuF.

The steps of AuF formation were carefully followed from FESEM results. A spontaneous assembly mechanism has been proposed from the time-course experimental condition. During the synthesis of AuFs the reaction was quenched time to time by taking out the resin beads (physical separation) from aqueous phase to relate the crystal growth and shape transformation. From FESEM study we see that the ~100 nm Cu(0) nanoparticles (Supporting Information, Figure 6) are embedded onto the resin surface as a result of $NaBH_4$ reduction of Cu(II). After that, addition of $HAuCl_4$ solution stimulates galvanic replacement. Initially $HAuCl_4$ promotes innumerable Au(0) nuclei on Cu(0) and the size of the particles increased to ~200 nm (Figure 6e). After 40 min of galvanic replacement reaction, we observed the spherical Cu(0) particle with rough surface due to the assembly of small Au(0) nuclei onto larger particles (Figure 6f). As the galvanic reaction progressed the Au(III) concentration decreased in solution and finally highly branched AuFs resulted in from the diffusion-related pathways (Figure 6g,h). Synthesized Au flowers show a double-humped DRS profile (Supporting Information, Figure 7).

dx.doi.org/10.1021/jp306330p | J. Phys. Chem. C 2012, 116, 24301–24313

Gold nanoparticles have been widely used as Raman active substrates because of biocompatibility, stability in comparison to other SERS active substrate. Single molecule detection by surface enhanced Raman scattering (SM-SERS) depends mainly on SERS active colloidal silver clusters with fractal nature. Such cluster synthesis is often complicated and are vulnerable to surface oxidation. These are serious obstacles of silver nanostructure for practical applications in SERS, particularly for probing single biomolecules in physiological environments. Considering large scattering cross section of 4-mercaptopyridine (4-MPy) molecule and well-defined monolayer coverage on gold surfaces, 4-MPy served well as a probe molecule for single molecule detection. The result stands superior to spherical gold nanospheres of variable size prepared by Frens' method.[28] A representative spectrum has been presented for a comparative account.

The adsorptive properties of the ligand 4-MPy molecules on the as-prepared AuF have been estimated. A simple yet elegant absorption spectroscopic technique as reported elsewhere[27] has been applied to understand the concentration of the ligand (here 4-MPy) actually adsorbed on AuF surface. For this purpose, 1.5 mg of AuF substrate was taken and mixed with four different concentrations of 4-Mpy in four different test tubes. The dispersed AuF−4Mpy mixtures were then incubated for 8 h. The supernatant was obtained after centrifugation and the UV−vis absorption spectra for each of the *as obtained* supernatant solution were recorded. The centrifugation process allows removal of the free ligand, leaving the adsorbed ligand molecules on the AuF. The UV−vis extinction spectra of the probe molecule at different concentrations were then compared with that of the filtrate obtained from AuF suspension containing the same concentration of the ligand. From these extinction spectra, the information regarding the concentration $[C]$ of the ligand in AuF solution and the concentration $[\Gamma]$ of the ligand actually adsorbed on the AuF surface are extracted and the results so obtained are then utilized to plot C/Γ versus C graph. From the slope and the intercept of the graph, the adsorptive parameters [ca. the adsorption coefficient (K) maximum adsorption, and free energy (ΔG)] were estimated. The information regarding the concentration $[C]$ of the ligand in AuF solution and the concentration $[\Gamma]$ of the ligand actually adsorbed on the AuF surface has been extracted from the absorption spectra, which are then utilized to plot C/Γ versus C graph shown in Figure 7. The points so obtained in the graph when fitted linearly show the typical shape of adsorption isotherm and they faithfully satisfy the following Langmuir equation:

$$C/\Gamma = 1/K\Gamma_{max} + C/\Gamma_{max} \quad (2)$$

where Γ_{max} represents the surface concentration at saturation of the active sites and K signifies the adsorption coefficient. From the above curve, the adsorption coefficient (K) of 4-MPy onto AuF is estimated to be $\sim 0.23 \times 10^6$ M^{-1}, corresponding to adsorption free energy (ΔG) $\sim$ 28.5 kJ M^{-1}.

The SERS spectra of 4-mercaptopyridine (4-MPy) molecule adsorbed on as prepared AuF at different concentrations of the adsorbate ranging from 1.0×10^{-7} M−1.0×10^{-12} M are shown in Figure 8. The NRS spectrum of the molecule at 0.1 M concentration in aqueous solution is also shown in Figure 8. The vibrational signatures of the 4-MPy molecule are well assigned and are reported in literatures.[28b,c] The spectra as shown in Figure 8 exhibit well-resolved, sharp, and enhanced Raman bands characteristic of 4-MPy molecule. Supporting

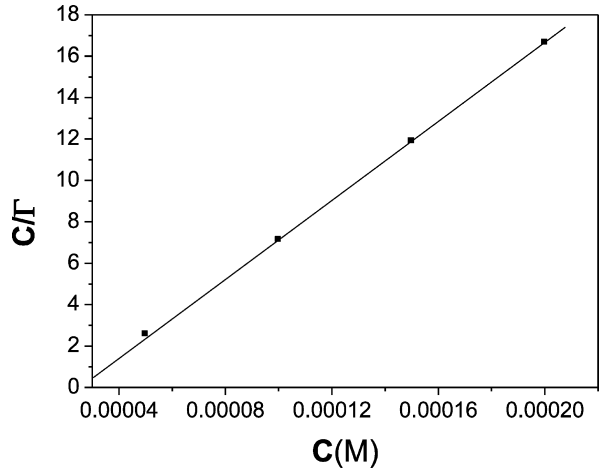

Figure 7. Experimental result of $[4\text{-MPy}]_{free}/[\text{AuF-4-MPy}]$ (C/Γ) vs $[4\text{-MPy}]_{free}$ (C) plot. The solid line represents the Langmuir linear regression fit of the experimental results.

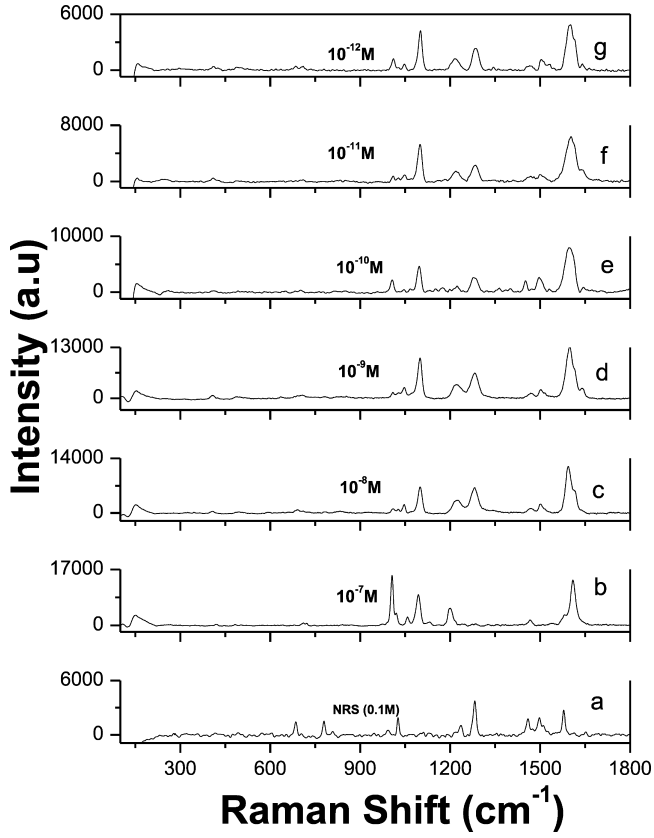

Figure 8. (a) NRS spectrum of 4-MPy at 0.1 M in aqueous solution and (b−g) SERS spectra of 4-MPy adsorbed on AuFs at various concentrations of the adsorbate for λ_{exc} = 632.8 nm.

Information, Figure 8 shows the FESEM image of a solid resin particle. We have presented NRS of resin and AuF without 4-MPy in order to ascertain whether these background signals influence the SERS signal of 4-MPy (Supporting Information, Figure 9). However, the spectra recorded at various adsorbate concentrations show different spectral profile. Structure of 4-MPy is susceptible to pH change.[29] Protection of ring N takes place only below pH = 2. The experimental pH remains well above 5.5 both before and after incubation of gold flower in 4-

dx.doi.org/10.1021/jp306330p | J. Phys. Chem. C 2012, 116, 24301−24313

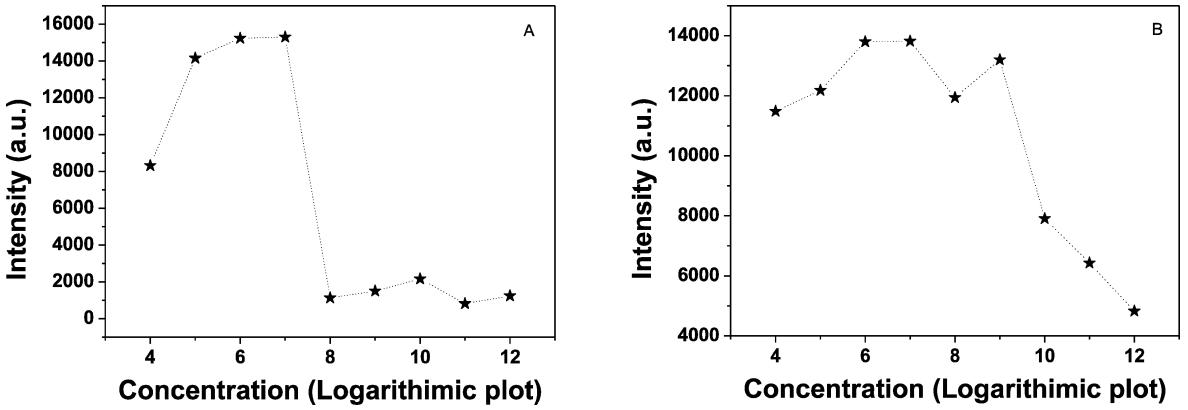

Figure 9. Shows the variation in SERS intensity of 1007 cm^{-1} (A) and 1584 cm^{-1} (B) bands with the change in concentrations of the 4-MPy molecule.

Table 1. Apparent Enhancement Factors (AEF) of some Selected Raman Bands of the 4-MPy Molecule Adsorbed on AuF Substrate[a]

NRS, 0.1 M (cm^{-1})	symmetry	assignment	SERS [10^{-7} M] (cm^{-1})	AEF × 10^7	SERS [10^{-8} M] (cm^{-1})	AEF × 10^8	SERS [10^{-10} M] (cm^{-1})	AEF × 10^{10}	SERS [10^{-12} M] (cm^{-1})	AEF × 10^{12}
			156 [ν_{Au-S}]		156 [ν_{Au-S}]		156 [ν_{Au-S}]		156 [ν_{Au-S}]	
991 (w)	A_1	ν_1 (ring breathing)	1005	2.18	1005	0.15	1005	0.32	1006	0.17
1024 (ms)			1024							
				cnm	1046	cnm	1044	cnm	1047	cnm
	A_1	$\beta_{(C-H)}$ring breathing (ν_{18})	1057	cnm						
1108 (vvw)	A_1	trigonal ring-breathing with C═S deformation (ν_{12})	1092	1.285	1097	2.15	1094	1. 52	1098	1.37
			1165	cnm		cnm		cnm		cnm
			1204	cnm		cnm		cnm		cnm
1216 (w/ sh)		$\beta_{(C-H)}$	1219	0.22	1222	0.54	1222	0.18	1222	0.2
1233 (w)										
1280 (vvs)	B_2	$\beta_{(C-H)}(\nu_3)$			1283	0.17	1281	0.07	1283	0.07
							1364	cnm		cnm
							1450	cnm		cnm
1460 (ms)	A_1	ν_{C-C}/ν_{C-N} (ν_3)								
			1471	cnm	1471	cnm			1470	cnm
1496 (ms)					1497	0.12	1497	0.14 × 10^{10}	1504	0.06
1510 (sh)										
1581 (sh)	B_2	ν_{C-C}	1585	0.12	1592	cnm	1598	cnm	1601	cnm
1611 (w)	B_2	ν_{C-C}	1610	7.0						
	A_1	$\nu_{C-C}(\nu_8)$			1619	cnm				

[a]vs, very strong; s, strong; ms, medium strong; w, weak; vw, very weak; vvw, very very weak; sh, shoulder; cnm, could not measure.

Mpy solution. So, protonation is redundant. The nature of the spectral profile changes because of concentration effect only.

As the concentration of the adsorbate changes from 1.0 × 10^{-7} M to 1.0 × 10^{-8} M, intensity reversal is noticed between the pair of totally symmetric vibrational signatures (A_1) centered at ∼1007 and 1099 cm^{-1}. The former band has been ascribed to the ring breathing (υ_1) vibrations, while the later has been assigned to the trigonal ring breathing vibrations (υ_{12}) involving C═S deformation mode. A similar conclusion can be drawn for the pair of bands at ∼1584 and 1607 cm^{-1}. Both of these bands have been ascribed to υ_{C-C} stretching vibrations (υ_8) belonging to B_2 irreducible representations. With the decrease in concentration of the adsorbate, the 1584 cm^{-1} band gains in intensity, significantly blue-shifted and appear as well-resolved intense band centered at ∼1600 cm^{-1}. The 1607 cm^{-1} band is also blue-shifted and appear as weak shoulder at ∼1618 cm^{-1}. Apart from the enhancement of the ring breathing and stretching modes, the SERS spectrum at 1.0 × 10^{-7} M concentration of the adsorbate is characterized by intense SER signals centered at ∼1200 cm^{-1} together with weak but prominent band at ∼1469 cm^{-1}. The 1200 cm^{-1} band is assigned to in-plane β (CH) mode and 1469 cm^{-1} represent totally symmetric $\upsilon_{C-C}/\upsilon_{C-N}$ stretching vibrations (υ_{19}) owing to A_1 irreducible representation. An interesting conclusion can be drawn regarding the well-resolved and distinct band at ∼1280 cm^{-1} in the SERS spectra of the molecule recorded in the concentration range 1.0 × 10^{-8}−1.0 × 10^{-12} M. This band is absent in the SERS spectrum at higher adsorbate

dx.doi.org/10.1021/jp306330p | J. Phys. Chem. C 2012, 116, 24301−24313

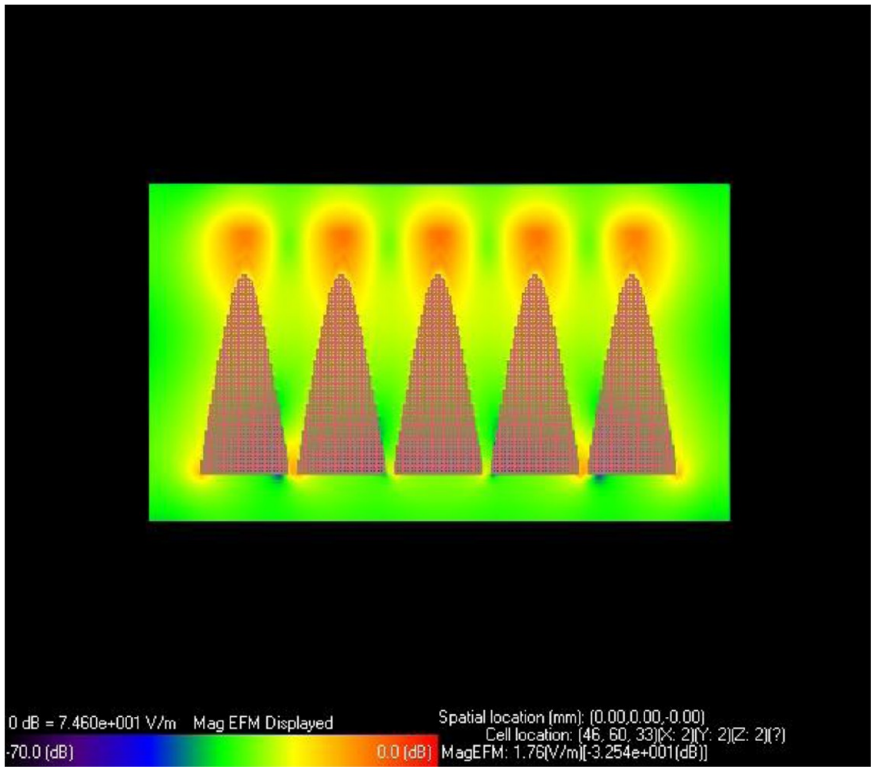

Figure 10. Snapshot of the 3D-FDTD simulated results showing the spatial distribution of the electric field around the nanotips of AuF.

concentration (ca. $\sim 1.0 \times 10^{-8}$ M) and has been assigned to in-plane β (CH) bending (υ_1) vibrations referring to B_2 irreducible representations. The variation in the relative and absolute intensities of the enhanced Raman bands in the concentration-dependent SERS spectra (Figure 8) may primarily be attributed to the change in orientation of the molecule.

The variation in SERS intensity with the change in concentrations of the 4-MPy molecule has been estimated. Figure 9 shows the plot of the variation in SER intensity of intense and well-resolved 1007 and 1584 cm^{-1} bands with the logarithm of concentration. It is observed that the SER signal increases as the concentration of the adsorbate molecule is lowered, maximizes at 1.0×10^{-6}–1.0×10^{-7} M and then decreases again with a further decrease in concentration. It is now well-established that, on silver island films and on nanocolloids,[30] maximum enhancement is observed when a monolayer of the adsorbate molecule is formed on the surface and that, as multilayers are formed, the SER signal decreases. It, therefore, seems plausible that the monolayer of the adsorbed 4-MPy molecule is formed on AuF at concentrations $\sim 1.0 \times 10^{-6}$–1.0×10^{-7} M, which shows maximum enhancement of the SER signal.

To have a precise idea regarding the orientation of the molecule, we estimate the apparent enhancement factors (AEFs) of some selected Raman bands using the relation we reported.[31]

Accordingly,

$$\mathrm{AEF} = \sigma_{\mathrm{SERS}}[C_{\mathrm{NRS}}]/\sigma_{\mathrm{NRS}}[C_{\mathrm{SERS}}] \quad (3)$$

where C and σ represent the concentration and the peak area of the Raman bands measured from baseline.

The AEF values of the enhanced Raman bands at various concentrations of the adsorbate are shown in Table 1. If the yz plane is considered to be the pyridyl ring plane of 4-MPy molecule, z corresponds to the C_2 axis, then for the edge on adsorption of the molecule, the vibration of the in-plane totally symmetric A_1 species spanning as zz are expected to endure the strongest enhancement. Modes of irreducible representations B_1 and B_2, transforming as xz and yz, respectively, will also be enhanced. The normal modes belonging to A_2 irreducible representation, transforming as xy should be least enhanced in the SERS spectra.

It is clearly seen from Table 1, that we obtain a significant 7–12 orders of magnitude enhancement of almost all the Raman bands principally representing the in-plane vibrations belonging to A_1 and B_2 symmetry species of the 4-MPy molecule. The as-prepared AuF thus act as a superior SERS active substrate compared to that of silver colloids, ZnS nanocrystals, nanotextured silver surface, and nanoflower substrate, as reported elsewhere.[27,32] No significant enhancements from the out-of-plane vibrations marked either by the A_2 or B_1 species are recorded. These results together with the appearance of the intense and broad band at ~ 157 cm^{-1} ascribed to ν(Au–S) vibration in the entire concentration-dependent SERS spectral profile, suggest that the 4-MPy molecules are adsorbed on the AuF surface through the sulfur (S) atom of the molecule with the molecular plane almost perpendicular to the surface. This conjecture is in accordance with the preceding reports pertaining to the adsorption behavior of 4-MPy molecules on ZnS nanocrystals, nanotextured silver surface and silver hydrosols. However, the relative variation in intensities and enhancement factors of the SERS bands at various concentrations of the adsorbate may indicate fluxional motion of the molecule on the colloidal AuF surface, yielding a distribution of edge-on absorptive stances.

To elucidate the genesis of huge enhancement of SERS signal of 4-MPy molecule adsorbed on AuF, the electric field

dx.doi.org/10.1021/jp306330p | J. Phys. Chem. C 2012, 116, 24301–24313

distribution around the extended nano tips of the AuF surface has been estimated. The spatial distribution of the electric field around the illuminated gold nano tips, as obtained from the 3D-FDTD simulation, is shown in Figure 10. It is clearly seen from the Figure 10, that the electric fields around the apex of the gold nano tips are remarkably higher. This is referred to as "lightning rod effect" which results in the generation of gigantic electric field.

The enhancement factor (G) of each molecule may be approximately represented by the following relation:

$$G(\omega, \omega') = |E(\omega)|^2 |E(\omega')|^2 \quad (4)$$

where, $E(\omega)$ is the local electric field enhancement at the incident frequency ω and $E(\omega')$ is the corresponding factor at the Stokes-shifted frequency ω'. From Figure 10, it is clearly seen that the magnitude of maximum enhancement of the electric field around the nano tips is ~74.6 V/m; which approximately corresponds to the enhancement as high as ~9 orders of magnitude in the SER signal of the 4-MPy molecule. Critical examination revealed that gold NFs showed ~25 times stronger SERS signal than that of SERS obtained from spherical AuNPs.[26] The comparative account has been given in Figure 11. Field enhancement due to the coupling effect is more than

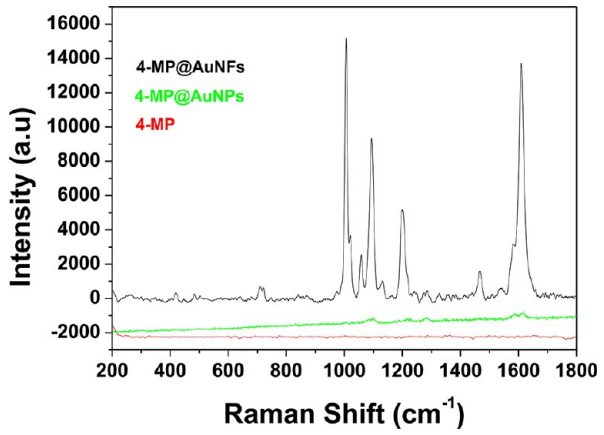

Figure 11. Comparative SERS signals obtained from aq. 4-MPy solution (10^{-7} M) involving 55 nm spherical AuNPs (green line) and AuFs (black line). NRS of aq 4-MPy solution (10^{-7} M) is indicated in red.

10^3 times larger for a pair of tip-to-tip nanostructure with a small gap in comparison to an isolated one. This will yield extremely intense near-field optical light sources with high local contrast that suits the improvement of SERS effect.[33] Unlike gold nanospheres, gold NFs have a coarse surface and dense tips, increased surface area, and a large numbers of "hot spots", those inculcate higher SERS enhancement.

However, ~10−12 orders of magnitude enhancements of almost all the experimentally observed SER bands belonging to the B_2 and A_1 symmetry species (vide supra and Table 1), presage considerable involvement of the charge transfer (CT) mechanism (in addition to the EM mechanism) to the overall SER enhancement of the molecule.

To comprehend the selective enhancement of the normal modes of vibrations of the 4-MPy molecule belonging to A_1 and B_2 symmetry species, the intensity of Raman transition in terms of the polarizability tensor elements as proposed by Albrecht has been considered. According to Albrecht,[34] the polarizabilty tensor elements which can perturb the intensity of Raman bands under resonance Raman (RR) conditions are expressed as

$$\alpha_{\sigma\rho} = A + B + C \quad (5)$$

The "A" term represents a Franck−Condon (FC) contribution, while the "B" and "C" terms are collectively designated as Herzberg−Teller (hereafter HT) contributions. A CT model for SERS, based on the theory of Albrecht has been proposed.[35] As in RR, the Raman polarizability tensor elements ($\alpha_{\sigma\rho}$) in SERS are also represented by the Albrecht's "A", "B", and "C" terms where σ and ρ represent the x, y, z directions in the Euclidean space. Only totally symmetric vibrational signatures in the SERS spectrum are expected to be enhanced by the "A" term. The HT contributions are considered to be responsible for the selective enhancement of the Raman bands via molecule to metal CT and metal to molecule CT, respectively[28d,36] Both totally and nontotally symmetric vibrational modes in the SERS spectrum may be enhanced by the Albrecht's "B" and "C" terms.[36] Term "A" in the case of metal to molecule CT from a filled Fermi level $|F\rangle$ of the metal to the excited molecular state $|K\rangle$ is represented by[28d]

$$A = (2/\hbar)\mu^{\sigma}_{FK}\mu^{\rho}_{FK}\langle i|k\rangle\langle k|f\rangle \frac{\omega_{FK} + \omega_f}{(\omega_{FK} + \omega_f)^2 - \omega^2} \quad (6)$$

where, μ^{σ}_{FK} and μ^{ρ}_{FK} represent the electronic transition dipole moments from the Fermi level $|F\rangle$ of the metal to the affinity level of the excited molecular state $|K\rangle$ along the σ and ρ directions, respectively, ω is the frequency of the exciting laser radiation, while ω_f and ω_{FK} represent the frequencies of vibration of the Fermi level of the metal, and the transition frequency between the Fermi level $|F\rangle$ of the metal to the excited state $|K\rangle$ of the molecule respectively. The $|i\rangle$, $|k\rangle$, and $|f\rangle$ represent vibrational wave functions of the corresponding vibronic states $|I\rangle$, $|K\rangle$, and $|F\rangle$. The Albrecht's A term is normally associated with resonance Raman spectroscopy and as the denominator strikes the resonance only then appreciable intensity is predicted. Far away from resonance excitation, the numerator vanishes, while on resonance, the numerator restricts the enhancement of those normal modes, which are totally symmetric. Because the excitation used in the experiment with 632.8 nm laser line is far away from the resonance excitation of electrons from the Fermi level of the metal to the affinity level of the adsorbate, the contribution from the Albrecht's A term toward the enhancement of SERS signal is small.[37a,38]

Interestingly, the SERS spectra of the molecule are characterized by the significant enhancements of Raman bands centered at ~1283, 1591, and 1610 cm^{-1}. Far from resonance excitation (as in the present case), the contribution from this term toward the enhancement of SERS signal may not be too appreciable.

This is further substantiated by the significant enhancement of Raman bands centered at ~1283, 1591, and 1610 cm^{-1} in the SERS spectra of the molecule. All these modes belong to nontotally symmetric B_2 irreducible representation. The enhancement of the B_2 modes in the SERS spectra, may primarily presage the CT effect of SERS through intensity borrowing from some allowed molecular transitions (the HT contribution) of the 4-MPy molecule.[28d] The direction of CT in the case of 4-MPy molecule adsorbed on AuF surface is from metal to molecule as predicted for other pyridine and pyridine derivative molecules adsorbed on various nanotextured SERS

active substrates.[28d,37] The Albrecht's "C" term thus alone represents the HT contribution toward the enhancement of SERS signal of the probe molecule.[28d,36] The modified Albrech "C" term, as proposed by Lombardi et al.[28d] to understand the CT mechanism of SERS, is represented as

$$C = -(2/\hbar^2) \sum_{K \neq I} \frac{[\mu_{KI}^{\sigma}\mu_{FK}^{\rho} + \mu_{KI}^{\rho}\mu_{FK}^{\sigma}](\omega_{KI}\omega_{FK} + \omega^2)h_{IF}\langle i|Q|f\rangle}{(\omega_{KI}^2 - \omega^2)(\omega_{FK}^2 - \omega^2)} \quad (7)$$

where $|i\rangle$ and $|f\rangle$ are the initial and final quanta of the normal mode Q and μ_{FK} represents the electronic transitions from the Fermi level $|F\rangle$ of the metal to the affinity level of the excited state $|K\rangle$ of the molecule. The transition is feasible through intensity borrowing from the allowed molecular transition $|I\rangle \rightarrow |K\rangle$, where $|I\rangle$ represent the ground vibronic state of the molecule. μ_{KI} denotes the transition dipole moment for the allowed transition from the ground vibronic state $|I\rangle$ to the excited vibronic state $|K\rangle$. The transition frequencies between $|F\rangle \rightarrow |K\rangle$ and $|I\rangle \rightarrow |K\rangle$ are represented by ω_{FK} and ω_{KI}, respectively, and ω signify the frequency of the incident laser beam. The term h_{IF} in the above expression is called the HT coupling constant.

For the "C" term to be nonvanishing, the terms $\langle i|Q|f\rangle$,h_{IF}, μ_{KI}, and μ_{FK} must be simultaneously nonzero, and this fundamental requirement leads to the HT surface selection rule. The simplified expression of the HT surface selection rule is expressed as[28d,38]

$$\Gamma(Q_K) = \sum_K \Gamma(\mu_{CT}^{\perp}) \times \Gamma_K \quad (8)$$

where, $\Gamma(Q_K)$ is the irreducible representation to which the SERS active vibrational signature belongs. $\Gamma(\mu_{CT}^{\perp})$ is the irreducible representation to which the component of the CT dipole moment perpendicular to the surface belongs in the combined molecule-metal system, and Γ_K is the irreducible representation of the molecular excited state to which the optical transition $|I\rangle \rightarrow |K\rangle$ is allowed. It is to be noted that the summation runs presumably on low lying optical transitions. If $\Gamma(\mu_{CT}^{\perp})$ is totally symmetric, the expression of the HT selection rule is further simplified as

$$\Gamma(Q_K) = \sum_K \Gamma_K \quad (9)$$

The absorption spectrum of the 4-MPy molecule, as shown in Figure 12a, is characterized by intense cathedral type absorption maxima at ~347 and 359 nm, with a flex at ~325 nm along with a distinct broad band at ~229 nm. With the increase in polarity of the solvent 347, 359, and 325 nm bands undergo hypsochromic shift. The peaks and the humps of the absorption maxima thus represent transitions typically of $n \rightarrow \pi^*$ type. The theoretically simulated absorption spectrum of the molecule is shown in Figure 12b. Table 2 shows the experimentally observed and theoretically predicted allowed transitions between the low lying electronic states of the 4-MPy molecule. The broad absorption maximum at ~229 nm may be considered to be due to the overlapping of strongly allowed transitions theoretically predicted at 223 and 225 nm. Both the theoretically simulated transitions at 223 and 225 nm correspond to $^1B_2$ symmetries with oscillator strengths (f) 0.1823 and 0.0495, respectively. The experimentally observed

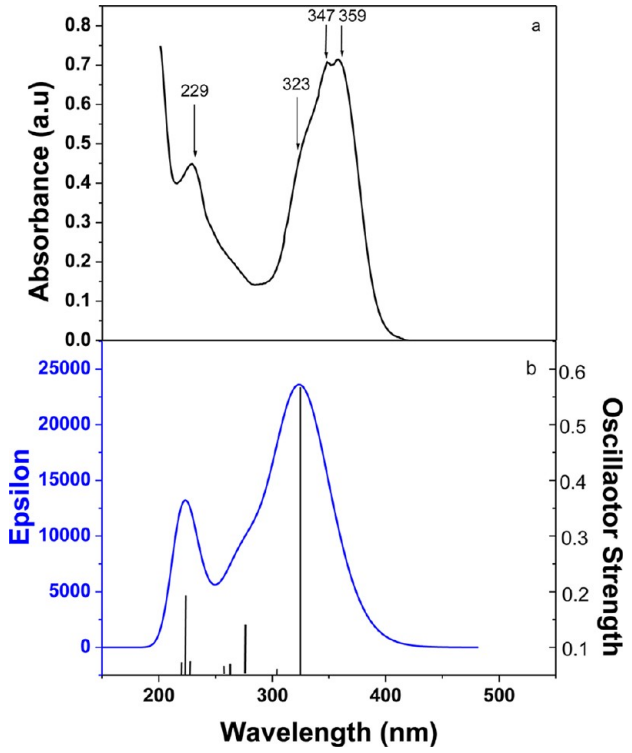

Figure 12. (a) Experimental and (b) theoretically simulated UV−vis spectra of 4-MPy.

Table 2. Experimental and Theoretical Absorption Value of 4-MPy Molecule

	λ_{max} (in nm)			
transition	expt	calcd	oscillator strength (f)	symmetry (C_{2v})
	229	223	0.1823	$^1B_2$
		225	0.0495	
$n \rightarrow \pi^*$	325	325	0.5584	$^1A_1$
$n \rightarrow \pi^*$	347	340	0.0002	$^1A_2$
$n \rightarrow \pi^*$	359			

hump at ~325 nm is also theoretically estimated at 325 nm corresponding to $^1A_1$ symmetries with oscillator strength (f) 0.5584. The HT selection rules are now applied which requires that the CT dipole moment operator ($\mu_{CT}^{\perp}$) be perpendicular to the surface. For the AuF-4-MPyy complex (considering its predefined orientation in space and C_{2v} point group symmetry), $\mu_{CT}^{\perp}$ belongs to the A_1 irreducible representation. Thus, the CT states according to HT selection rules must be of B_2 and A_1 symmetries ($\Gamma(Q_K) = A_1 \otimes B_2 = B_2$ and $\Gamma(Q_K) = A_1 \otimes A_1 = A_1$) corresponding to the UV transitions at 229 and 325 nm, respectively. The HT intensity borrowing from a strongly allowed $^1B_2 \leftarrow {}^1A_1$ ($n \rightarrow \pi^*$) and $^1A_1 \leftarrow {}^1A_1$ ($n \rightarrow \pi^*$) transitions, in turn allow the normal modes of vibrations belonging to the B_2 and A_1 irreducible representations in the SERS spectra, to be enhanced significantly via the contribution from the Albrecht's C term. Thus, the enhancement of SER bands at ~1280, 1584, and 1607 cm^{-1}, all belonging to B_2 irreducible representations, may be accounted for the CT contribution via the Albrecht's C term. The selective and substantial enhancement of the B_2 modes in the SERS spectra is indeed reported to be associated with the chemical properties of the molecule and could not be explained by the EM models.[21]

dx.doi.org/10.1021/jp306330p | J. Phys. Chem. C 2012, 116, 24301−24313

The experimentally observed hump at ∼325 nm is also theoretically estimated at 325 nm corresponding to $^1A_1$ symmetries with oscillator strength (f) 0.5584. The allowed optical transition at 325 nm (vide supra) is associated with strong oscillator strength (f = 0.5584). Hence, the overall enhancement of SER bands at ∼1007, 1099, 1200, and 1469 cm^{-1} of the 4-MPy molecule, belonging to the totally symmetric A_1 species, may result from the active involvement of the Albrecht's C term, from the weak but definite involvement of Albrecht's A term and the rest from the enhancement of the electromagnetic field due to the coupling of the localized surface plasmons.

CONCLUSIONS

In conclusion, it has become first-hand information to produce highly branched Au flowers that are quite stable for a long time (over months together). We are able to fabricate a carnation flower like structure of gold substrate (AuF) by subtle manipulation of the redox couple (Cu(0)/$HAuCl_4$). The manifestation happens under moderate but simple hydrothermal reaction (∼90 °C) conditions, varied precursor concentrations, and controlled EFF of the charged polystyrene beads as a solid support. This process provides a locally high growth rate and facilitates the formation of branched nanocrystals via overgrowth. It explains how the galvanic replacement process can be used to modulate growth kinetics. The process elaborates the scope of redox couples for other nanostructured material syntheses for different applications. The electric field distributions around the representative nanotips of AuF have been estimated from 3D-FDTD simulation studies. The concentration-dependent SERS spectra of the 4-MPy molecule adsorbed on as-synthesized AuF have been recorded. Significant 7−12 orders of magnitude enhancement of almost all the Raman bands principally representing the in-plane vibrations belonging to A_1 and B_2 symmetry species of the 4-MPy molecule have been estimated. The selective enhancements of the SER bands of the molecule have been unveiled from the view of Herzberg−Teller (HT) CT mechanism. Once again, the importance of "hot spot" and "naked" hierarchical structure for SERS is publicized.

ASSOCIATED CONTENT

Supporting Information

EDX, XRD, and UV−vis spectroscopic study of synthesized AuF. FESEM image of worm-like Au nanostructure, mixture of CuO polyhedral and Au flower, FESEM image of solid resin bead and Cu(0) nanoparticles on resin bead. SERS spectra of 4-MPy from fresh and aged substrates. NRS of resin beads and AuF without 4-MPy. This material is available free of charge via the Internet at http://pubs.acs.org.

AUTHOR INFORMATION

Notes

The authors declare no competing financial interest.

ACKNOWLEDGMENTS

BRNS Bombay, CSIR, and DST New Delhi are acknowledged for financial assistance and Indian Institute of Technology, Kharagpur, is acknowledged for research facilities.

REFERENCES

(1) Sanders, A. W.; Routenberg, D. A.; Wiley, B. J.; Xia, Y.; Dufresne, E. R.; Reed, M. A. Observation of Plasmon Propagation, Redirection, and Fan-Out in Silver Nanowires. *Nano Lett.* **2006**, *6*, 1822.

(2) Chen, S.; Yang, Y. Magnetoelectrochemistry of Gold Nanoparticle Quantized Capacitance Charging. *J. Am. Chem. Soc.* **2002**, *124*, 5280.

(3) Li, Y.; Hong, X. M.; Collard, D. M.; El-Sayed, M. A. Suzuki Cross-Coupling Reactions Catalyzed by Palladium Nanoparticles in Aqueous Solution. *Org. Lett.* **2000**, *2*, 2385.

(4) Sau, T. K.; Murphy, C. J. Seeded High Yield Synthesis of Short Au Nanorods in Aqueous Solution. *Langmuir* **2004**, *20*, 6414.

(5) (a) Lu, L.; Ai, K.; Ozaki, Y. Environmentally Friendly Synthesis of Highly Monodisperse Biocompatible Gold Nanoparticles with Urchin-like Shape. *Langmuir* **2008**, *24*, 1058. (b) Yuan, H.; Ma, W.; Chen, C.; Zhao, J.; Liu, J.; Zhu, H.; Gao, X. Shape and SPR Evolution of Thorny Gold Nanoparticles Promoted by Silver Ions. *Chem. Mater.* **2007**, *19*, 1592. (c) Wang, C.; Wang, T.; Ma, Z.; Su, Z. pH-Tuned Synthesis of Gold Nanostructures from Gold Nanorods with Different Aspect Ratios. *Nanotechnology* **2005**, *16*, 2555.

(6) (a) Hao, F.; Nehl, C. L.; Hafner, J. H.; Nordlander, P. Plasmon Resonances of a Gold Nanostar. *Nano Lett.* **2007**, *7*, 729. (b) Wang, Y.; Camargo, P. H. C.; Skrabalak, S. E.; Gu, H.; Xia, Y. A Facile, Water-Based Synthesis of Highly Branched Nanostructures of Silver. *Langmuir* **2008**, *24*, 12042. (c) Xiangqin, Z.; Erbo, Y.; Shaojun, D. Seed-Mediated Synthesis of Branched Gold Nanoparticles with the Assistance of Citrate and Their Surface-Enhanced Raman Scattering Properties. *Nanotechnology* **2006**, *17*, 4758.

(7) Rashid, M. H.; Bhattacharjee, R. R.; Kotal, A.; Mandal, T. K. Synthesis of Spongy Gold Nanocrystals with Pronounced Catalytic Activities. *Langmuir* **2006**, *22*, 7141.

(8) (a) Kneipp, J.; Kneipp, H.; Kneipp, K. SERS−A Single-Molecule and Nanoscale Tool for Bioanalytics. *Chem. Soc. Rev.* **2008**, *37*, 1052. (b) Lim, D. -K.; Jeon, K. -S.; Kim, H. M.; Nam, J. -M.; Suh, Y. D. Nanogap-Engineerable Raman-Active Nanodumbbells for Single-Molecule Detection. *Nat. Mater.* **2010**, *9*, 60.

(9) Hu, J.; Chen, M.; Fang, X.; Wu, L. Fabrication and Application of Inorganic Hollow Spheres. *Chem. Soc. Rev.* **2011**, *40*, 5472.

(10) Sun, Y.; Wang, Y. Monitoring of Galvanic Replacement Reaction between Silver Nanowires and $HAuCl_4$ by In Situ Transmission X-ray Microscopy. *Nano Lett.* **2011**, *11*, 4386.

(11) Ortiz, N.; Skrabalak, S. E. Controlling the Growth Kinetics of Nanocrystals via Galvanic Replacement: Synthesis of Au Tetrapods and Star-Shaped Decahedra. *Cryst. Growth Des.* **2011**, *11*, 3545.

(12) (a) Khoury, C. G.; Vo-Dinh, T. Gold Nanostars For Surface-Enhanced Raman Scattering: Synthesis, Characterization and Optimization. *J. Phys. Chem. C* **2008**, *112*, 18849. (b) Yuan, H.; Khoury, C. G.; Hwang, H.; Wilson, C. M.; Grant, G. A.; Vo-Dinh, T. *Nanotechnology* **2012**, *23*, 075102.

(13) Tian, Z. -Q.; Ren, B.; Wu, D. -Y. Surface-Enhanced Raman Scattering: From Noble to Transition Metals and from Rough Surfaces to Ordered Nanostructures. *J. Phys. Chem. B* **2002**, *106*, 9463.

(14) Liu, R.; Liu, J. -F.; Zhou, X. -X.; Sun, M. -T.; Jiang, G. -B. Fabrication of a Au Nanoporous Film by Self-Organization of Networked Ultrathin Nanowires and Its Application as a Surface-Enhanced Raman Scattering Substrate for Single-Molecule Detection. *Anal. Chem.* **2011**, *83*, 9131.

(15) (a) Hao, E.; Bailey, R. C.; Schatz, G. C.; Hupp, J. T.; Li, S. Synthesis and Optical Properties of "Branched" Gold Nanocrystals. *Nano Lett.* **2004**, *4*, 327. (b) Bakr, O. M.; Wunsch, B. H.; Stellacci, F. High-Yield Synthesis of Multibranched Urchin-Like Gold Nanoparticles. *Chem. Mater.* **2006**, *18*, 3297.

(16) Chen, S.; Wang, Z. L.; Ballato, J.; Foulger, S. H.; Carroll, D. L. Monopod, Bipod, Tripod, and Tetrapod Gold Nanocrystals. *J. Am. Chem. Soc.* **2003**, *125*, 16186.

(17) Xie, J.; Zhang, Q.; Lee, J. Y.; Wang, D. I. C. The Synthesis of SERS-Active Gold Nanoflower Tags for In Vivo Applications. *ACS Nano* **2008**, *2*, 2473.

(18) Sau, T. K.; Murphy, C. J. Room Temperature, High-Yield Synthesis of Multiple Shapes of Gold Nanoparticles in Aqueous Solution. *J. Am. Chem. Soc.* **2004**, *126*, 8648.
(19) Huang, L.; Wang, M.; Zhang, Y.; Guo, Z.; Sun, J.; Gu, N. Synthesis of Gold Nanotadpoles by a Temperature-Reducing Seed Approach and the Dielectrophoretic Manipulation. *J. Phys. Chem. C* **2007**, *111*, 16154.
(20) (a) Kunz, K.; Luebbers, R. *The Finite Difference Time Domain Method for Electromagnetics*; CRC Press: New York, 1993. (b) Fang, P.-P.; Li, J.-F.; Yang, Z.-L.; Li, L.-M.; Ren, B.; Tian, Z.-Q. Optimization of SERS Activities of Gold Nanoparticles and Gold-Core−Palladium-Shell Nanoparticles by Controlling Size and Shell Thickness. *J. Raman Spectrosc.* **2008**, *39*, 1679. (c) Tian, Z.-Q.; Yang, Z.-L.; Ren, B.; Li, J.-F.; Zhang, Y.; Lin, X.-F.; Hu, J.-W.; Wu, D.-Y. Surface-Enhanced Raman Scattering from Transition Metals with Special Surface Morphology and Nanoparticle Shape. *Faraday Discuss.* **2006**, *132*, 159.
(21) Pande, S.; Chowdhury, J.; Pal, T. Understanding the Enhancement Mechanisms in the Surface-Enhanced Raman Spectra of the 1,10-Phenanthroline Molecule Adsorbed on a Au@Ag Bimetallic Nanocolloid. *J. Phys. Chem. C* **2011**, *115*, 10497.
(22) Cances, E.; Mennucci, B.; Tomasi, J. A New Integral Equation Formalism for the Polarizable Continuum Model: Theoretical Background and Applications to Isotropic and Anisotropic Dielectrics. *J. Chem. Phys.* **1997**, *107*, 3032.
(23) (a) Maye, M. M.; Chun, S. C.; Han, L.; Rabinovich, D.; Zhong, C. -J. Novel Spherical Assembly of Gold Nanoparticles Mediated by a Tetradentate Thioether. *J. Am. Chem. Soc.* **2002**, *124*, 4958. (b) Wang, W; Yang, W.; Cui, X.; Growth, H. Mechanism of Flowerlike Gold Nanostructures: Surface Plasmon Resonance (SPR) and Resonance Rayleigh Scattering (RRS) Approaches to Growth Monitoring. *J. Phys. Chem. C* **2008**, *112*, 16348. (c) Guo, S.; Dong, S.; Wang, E. Monodisperse Raspberry-Like Gold Submicrometer Spheres: Large-Scale Synthesis and Interface Assembling for Colloid Sphere Array. *Cryst. Growth Des.* **2008**, *8*, 3581. (d) Zhao, L.; Ji, X.; Sun, X.; Li, J.; Yang, W.; Peng, X. Formation and Stability of Gold Flowers by the Seeding Approach: The Effect of Intraparticle Ripening. *J. Phys. Chem. C* **2009**, *113*, 16645.
(24) (a) Kedia, A.; Kumar, P. S. Precursor-Driven Nucleation and Growth Kinetics of Gold Nanostars. *J. Phys. Chem. C* **2012**, *116*, 1679. (b) Khoury, C. G.; Vo-Dinh, T. Gold Nanostars For Surface Enhanced Raman Scattering: Synthesis, Characterization and Optimization. *J. Phys. Chem. C* **2008**, *112*, 18849.
(25) (a) Jana, S.; Pande, S.; Sinha, A. K.; Sarkar, S.; Pradhan, M.; Basu, M.; Negishi, Y.; Pal, A.; Pal, T. Layer-by-Layer Deposition of Silver/Gold Nanoparticles for Catalytic Reduction of Nitroaromatics. *J. Nanosci. Nanotechnol.* **2010**, *10*, 847. (b) Sinha, A. K.; Basu, M.; Sarkar, S.; Pradhan, M.; Pal, T. Electrostatic Field Force Directed Gold Nanowires from Anion Exchange Resin. *Langmuir* **2010**, *26*, 17419.
(26) Frens, G. Controlled Nucleation for the Regulation of the Particle Size in Monodisperse Gold Suspensions. *Nat. Phys. Sci.* **1973**, *241*, 20.
(27) Muniz-Miranda, M.; Sbrana, G. Quantitative Determination of the Surface Concentration of Phenazine Adsorbed on Silver Colloidal Particles and Relationship with the SERS Enhancement Factor. *J. Phys. Chem. B* **1999**, *103*, 10639.
(28) (a) Wang, Y.; Sun, Z.; Hu, H.; Jing, S.; Zhao, B.; Xu, W.; Zhao, C.; Lombardi, J. R. Raman Scattering Study of Molecules Adsorbed on ZnS Nanocrystals. *J. Raman Spectrosc.* **2007**, *38*, 34. (b) Baldwin, J. A.; Vlckova, B.; Andrews, M. P.; Butler, I. S. Surface-Enhanced Raman Scattering of Mercaptopyridines and Pyrazinamide Incorporated in Silver Colloid-Adsorbate Films. *Langmuir* **1997**, *13*, 3744. (c) Baldwin, J.; Schuhler, N.; Butler, I. S.; Andrews, M. P. Integrated Optics Evanescent Wave Surface Enhanced Raman Scattering (IO-EWSERS) of Mercaptopyridines on a Planar Optical Chemical Bench: Binding of Hydrogen and Copper Ion. *Langmuir* **1996**, *12*, 6389. (d) Lombardi, J. R.; Birke, R. L. A Unified Approach to Surface-Enhanced Raman Spectroscopy. *J. Phys. Chem. C* **2008**, *112*, 5605.
(29) (a) Yu, H.-Z.; Xia, Nan.; Liu, Z.-F. SERS Titration of 4-Mercaptopyridine Self-Assembled Monolayers at Aqueous Buffer/Gold Interfaces. *Anal. Chem.* **1999**, *71*, 1354. (b) Hu, J.; Zhao, B.; Xu, W.; Li, B.; Fan, Y. Surface-Enhanced Raman Spectroscopy Study on the Structure Changes of 4-Mercaptopyridine Adsorbed on Silver Substrates and Silver Colloids. *Spectrochim. Acta, Part A* **2002**, *58*, 2827.
(30) (a) Sanda, P. N.; Warlaumont, J. M.; Dermuth, J. E.; Tsang, J. C.; Christmann, K.; Bradley, J. A. Surface-Enhanced Raman Scattering from Pyridine on Silver(111). *Phys. Rev. Lett.* **1980**, *45*, 1519. (b) Chowdhury, J.; Ghosh, M. Concentration-Dependent Surface-Enhanced Raman Scattering of 2-Benzoylpyridine Adsorbed on Colloidal Silver Particles. *J. Colloid Interface Sci.* **2004**, *277*, 121. (c) Chandra, S.; Chowdhury, J.; Ghosh, M.; Talapatra, G. B. Adsorption of 3-Thiophene Carboxylic Acid on Silver Nanocolloids. FTIR, Raman, and SERS Study Aided by Density Functional Theory. *J. Phys. Chem. C* **2011**, *115*, 14309.
(31) Pande, S.; Jana, S.; Sinha, A. K.; Sarkar, S.; Basu, M.; Pradhan, M.; Pal, A.; Chowdhury, J.; Pal, T. Dopamine Molecules on Aucore-Agshell Bimetallic Nanocolloids: Fourier Transform Infrared, Raman, And Surface-Enhanced Raman Spectroscopy Study Aided by Density Functional Theory. *J. Phys. Chem. C* **2009**, *113*, 6989.
(32) (a) Wang, Z.; Rothberg, L. J. Silver Nanoparticle Coverage Dependence of Surface-Enhanced Raman Scattering. *Appl. Phys. B: Laser Opt.* **2006**, *84*, 289. (b) Wang, Z.; Rothberg, L. J. Origins of Blinking in Single-Molecule Raman Spectroscopy. *J. Phys. Chem. B* **2005**, *109*, 3387. (c) Jiang, Y.; Wu, X.-J.; Li, Q.; Li, J.; Xu, D. Facile Synthesis of Gold Flowers with High Surface-Enhanced Raman Scattering Activity. *Nanotechnology* **2011**, *22*, 385601.
(33) Schuck, P. J.; Fromm, D. P.; Sundaramurthy, A.; Kino, G. S.; Moerner, W. E. Improving the Mismatch between Light and Nanoscale Objects with Gold Bowtie Nanoantennas. *Phys. Rev. Lett.* **2005**, *94*, 017402.
(34) Albrecht, A. C. On the Theory of Raman Intensities. *J. Chem. Phys.* **1961**, *34*, 1476.
(35) Lombardi, J. R.; Birke, R. L.; Lu, T.; Xu, J. Charge-Transfer Theory of Surface Enhanced Raman Spectroscopy: Herzberg−Teller Contributions. *J. Chem. Phys.* **1986**, *84*, 4174.
(36) Osawa, M.; Matsuda, N.; Yoshii, K.; Uchida, I. Charge Transfer Resonance Raman Process in Surface-Enhanced Raman Scattering from *p*-Aminothiophenol Adsorbed on Silver: Herzberg−Teller Contribution. *J. Phys. Chem.* **1994**, *98*, 12702.
(37) (a) Lombardi, J. R.; Birke, R. L. A Unified View of Surface-Enhanced Raman Scattering. *Acc. Chem. Res.* **2009**, *42*, 734. (b) Arenas, J. F.; Lopez-Tocon, I.; Centeno, S. P.; Soto, J.; Otero, J. C. How a Resonant Charge Transfer Mechanism Determines the Relative Intensities in the SERS Spectra of 4-Methylpyridine. *Vib. Spectrosc.* **2002**, *29*, 147. (c) Arenas, J. F.; Soto, J.; Pelaez, D.; Fernandez, D. J.; Otero, J. C. Understanding Complex Surface-Enhanced Raman Scattering, Using Quantum Chemical Calculations. *Int. J. Quantum Chem.* **2005**, *104*, 681. (d) Birke, R. L.; Znamenskiy, V.; Lombardi, J. R. a Charge-Transfer Surface Enhanced Raman Scattering Model from Time-Dependent Density Functional Theory Calculations on a Ag_{10}−Pyridine Complex. *J. Chem. Phys.* **2010**, *132*, 214707. (e) Fu, X.; Pan, Y.; Wang, X.; Lombardi, J. R. Quantum Confinement Effects on Charge-Transfer between PbS Quantum Dots and 4-Mercaptopyridine. *J. Chem. Phys.* **2011**, *134*, 024707.
(38) Cañamares, M. V.; Chenal, C.; Birke, R. L.; Lombardi, J. R. DFT, SERS, and Single-Molecule SERS of Crystal Violet. *J. Phys. Chem. C* **2008**, *112*, 20295.